Catalysis Today 240 (2015) 146–152

Contents lists available at ScienceDirect

Catalysis Today

journal homepage: www.elsevier.com/locate/cattod

Photocatalytic and electrooxidation properties of TiO_2 thin films deposited by sol–gel

G. Kenanakis[a,b], D. Vernardou[a], A. Dalamagkas[a], N. Katsarakis[a,b,*]

[a] Center of Materials Technology and Photonics, School of Applied Technology, Technological Educational Institute of Crete, 710 04 Heraklion, Crete, Greece
[b] Institute of Electronic Structure and Laser, Foundation for Research & Technology-Hellas, P.O. Box 1385, Vassilika Vouton, 711 10 Heraklion, Crete, Greece

ARTICLE INFO

Article history:
Received 20 January 2014
Received in revised form 11 April 2014
Accepted 11 May 2014
Available online 4 July 2014

Keywords:
TiO_2, Thin films
Sol–gel technique
Photocatalysis
Octadecanoic acid
Methanol oxidation

ABSTRACT

Anatase TiO_2 thin films are deposited on glass using alcoholic solutions at 400–600 °C. The effect of film thickness, grain size and annealing temperature on the catalytic activity of the TiO_2 thin films is investigated regarding the degradation of octadecanoic (stearic) acid under UV-A light illumination. Specifically, the photocatalytic activity of 150-nm-thick TiO_2 thin films deposited on glass at 500 °C is quite remarkable, showing the highest octadecanoic acid disappearance rate, i.e., 6.28×10^{-8} mol/min (formal quantum efficiency = 6.65×10^{-3}) at 30 min of UV-A light illumination. Moreover, the electrochemical performance of the same sample is evaluated by studying the electrocatalytic oxidation of methanol in an alkaline medium in dark and under UV illumination. Under UV illumination, the methanol electrooxidation is significantly improved, as evidenced by the current–potential measurements presenting a satisfactory incident photon to charge carrier efficiency of 88.3% with a fill factor of 0.51.

1. Introduction

Titanium dioxide (TiO_2) is one of the most highly studied metal oxides because of its interesting electrochemical and photocatalytic properties that are widely applied in photocatalysis, fuel cells, etc. [1–4]. TiO_2 nanopowders exhibit a high photocatalytic efficiency and mostly been used in small-scale purification systems. This is due to the energy acquisition of the procedure [huge amount of contaminant (water/air) necessitates high amounts of light energy], separation and recovery difficulties of the remained solid precipitate, which limit the extent of their technological applications. Supporting photocatalytic materials on a steady substrate can help overcoming this issue, targeting the decomposition of organic substances originally adsorbed on the surfaces [5,6].

In this work, we study the photocatalytic and electrooxidation properties of TiO_2 thin films, deposited via a sol–gel procedure on Corning and indium tin oxide (ITO) glass substrates and annealed at 400–600 °C. Based on the previous reports [7–9], we focused on examining the effect of film thickness, grain size and annealing temperature on the photocatalytic activity of octadecanoic acid. Moreover, the performance of the films toward the electrooxidation of methanol is tested by cyclic voltammetry in dark and under UV illumination. We provide evidence that the TiO_2 thin films exhibit promising photocatalytic and electrooxidation properties without the use of metals such as Pt or dopants such as N making the approach simpler, easier and environmental-friendly.

2. Experimental details

2.1. Reagents

The following chemical compounds were used: absolute ethanol (≥99.8%), hydrochloric acid (37%), titanium tetraisopropoxide ($Ti(OCH(CH_3)_2)_4$, ≥99.999%), octadecanoic acid ($CH_3(CH_2)_{16}COOH$, ≥98.5%), sulfuric acid (H_2SO_4, 95.0–98.0%), hydrogen peroxide (H_2O_2, 30 wt. % in H_2O), isopropanol (≥99.5%) and acetone (≥99.9%), all provided from Sigma-Aldrich. All reagents were used without further purification.

2.2. Preparation of glass substrates

Standard $10 \times 10\,mm^2$ Corning Eagle 2000 Borosilicate Glass (Specialty Glass Products) substrates (for the photocatalysis part) were used, along with ITO-coated glass slides (for the electrocatalytic measurements) with a surface resistivity of 8–12 Ω/sq

* Corresponding author at: Institute of Electronic Structure and Laser, Foundation for Research & Technology-Hellas, P.O. Box 1385, Vassilika Vouton, 711 10 Heraklion, Crete, Greece. Tel.: +30 2810 379703; fax: +30 2810 391305.
E-mail addresses: katsan@iesl.forth.gr, katsan@staff.teicrete.gr (N. Katsarakis).

http://dx.doi.org/10.1016/j.cattod.2014.05.007
0920-5861/

(Aldrich). Before deposition, the Corning glass substrates were cleaned for 10 min using a piranha solution (H_2SO_4/H_2O_2 = 3/1), rinsed with ultrapure water (18.2 MΩ cm) and dried under N_2 gas flow, while the ITO substrates were ultrasonically cleaned with isopropanol and acetone, washed with ultrapure water and dried under a N_2 gas flow.

2.3. Deposition of TiO_2 thin films

TiO_2 thin films with a thickness in the range of 50–150 nm were deposited on glass substrates using the sol–gel/spin coating technique reported elsewhere [10–12]. In particular, 2.8 ml of $Ti(OCH(CH_3)_2)_4$ was first dissolved in 25 ml of absolute ethanol. The resultant solution was stirred for 15 min at 60 °C using a magnetic stirrer to yield a homogeneous, clear and transparent solution. Five drops of concentrated hydrochloric acid were added in order to get an acidic solution, as proposed by Rampaul et al. [13], and avoid precipitation [14] (changing the pH value of the precursor solution from ~8.5–9.0 to ~1.25–1.75). The deposition was usually performed within 24 h after the solution was prepared, by spin-coating the substrates at 3000 rpm for 20 s [16,17]. After processing, the substrates were heated at 350 °C for 10 min to evaporate the solvent and remove the organic residuals from the films. This procedure was repeated up to four times. The films were then annealed in air at 400–600 °C for 120 min. The thickness of the films was measured using a stylus profilometer (alpha-step 100, Tencor).

2.4. Characterization techniques

The crystal structure of all samples was determined by X-ray diffraction (XRD) using a Rigaku (RINT 2000) diffractometer with Cu Ka X-rays, while their surface morphology was studied by means of a field emission scanning electron microscope (FE-SEM, JEOL JSM-7000F) and an atomic force microscope (AFM) in tapping mode (Digital Instruments Nanoscope IIIa). The surface roughness (RMS) of the TiO_2 thin films was determined using the scanning probe image processor (SPIP, v. 3.3.5.0) image processing software for nano- and micro-scale microscopy from Image Metrology. Finally, UV–Vis transmission spectra were recorded using a Perkin Elmer (Lambda 950) spectrophotometer over the wavelength range 190–1100 nm.

2.5. Photocatalytic activity study

There are many different methods that can be used to determine the activity of photocatalytic surfaces. Popular techniques include those based on the photo-oxidation of organic films such as octadecanoic (stearic) acid [15–20], or organic vapors [21] and contact angle changes [22].

The photocatalytic activity of our TiO_2 thin films was determined using octadecanoic acid as a model compound, in which a thin layer of octadecanoic acid is deposited onto the examined sample and its photocatalytic destruction is monitored as a function of time [15–20]. This method has gained preference over the years since it is simple to set up and run and needs no dedicated equipment beyond a standard laboratory FT-IR spectrometer. Since octadecanoic acid is a solid at room temperature, it is more easily controlled than a solution or gas, while it also provides a reasonable model for typical organic surface contamination that deposit on exterior and interior surfaces [23]. Moreover, octadecanoic acid is normally found in natural greases and thus is a convenient test material for the simulation of oil removal from the surface of coatings [24]. Furthermore, octadecanoic acid is very stable under UV illumination in the absence of a photocatalyst film (phenomenon of photolysis). Finally, octadecanoic acid can easily be laid down from a methanol or chloroform solution making the study much easier. In our case, a solution of 0.1 M octadecanoic acid in chloroform was spin-coated on the sample under test at a rotation speed of 500 rpm for 30 s. Samples were then dried at 80 °C in air for 10 min.

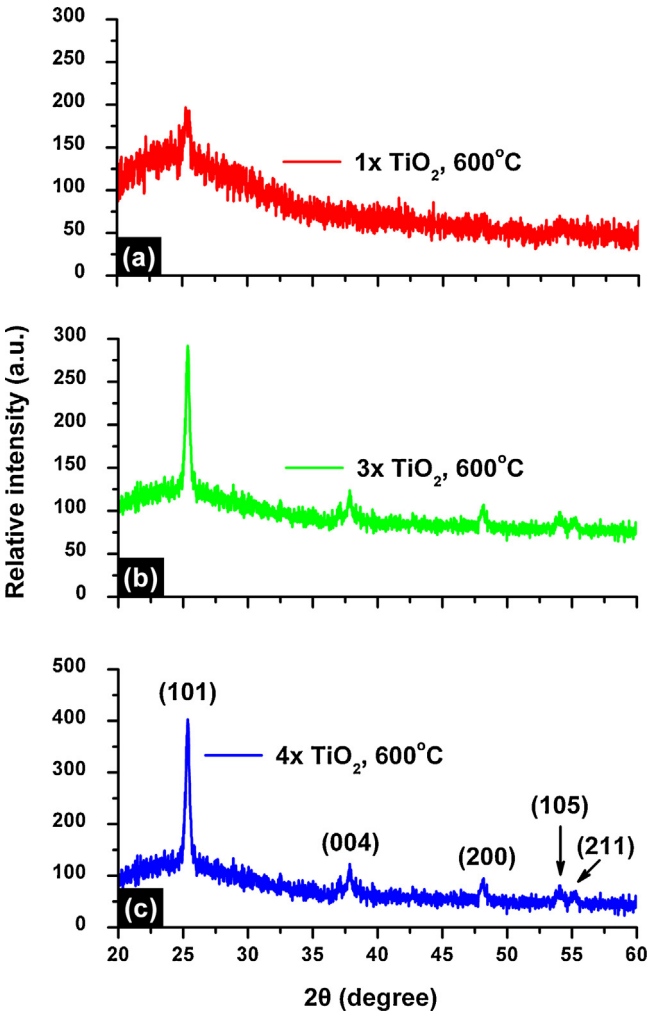

Fig. 1. X-ray diffraction patterns of the TiO_2 thin films deposited by a sol–gel/spin-coating procedure after 1 (a), 3 (b) and 4 (c) spinning cycles at 600 °C.

The decomposition of octadecanoic acid was demonstrated by FT-IR spectroscopy (FT-IR, IRPrestige-21, Shimadzu) through the monitoring of the asymmetric C–H stretching mode of the CH_3 group at 2958 cm^{-1} and the asymmetric and symmetric C–H stretching modes of the CH_2 group at 2923 and 2853 cm^{-1}, respectively. The photocatalytic activity experiments on all TiO_2 samples for the decomposition of octadecanoic acid were performed in ambient air and were repeated for five times demonstrating no changes in the % octadecanoic acid conversion. The integrated area (2800–3000 cm^{-1}) of the octadecanoic acid C–H stretching peaks was monitored before and after black light illumination in a box reactor at certain time intervals. The light source used was a HPK 125 W Philips mercury lamp with main emission wavelength at 365 nm and an incident light intensity of 8.9 mW/cm^2. For ease in comparison of the photocatalytic activity between different samples, the integrated area of the C–H stretching peaks measured at each irradiation time interval was normalized to the initial integrated area (prior to the irradiation) in order to calculate the percentage of octadecanoic acid remaining as a function of irradiation time. Blank experiments (photolysis) were also performed using bare glass substrates under exactly the same conditions applied for the TiO_2 samples. Finally, the octadecanoic acid

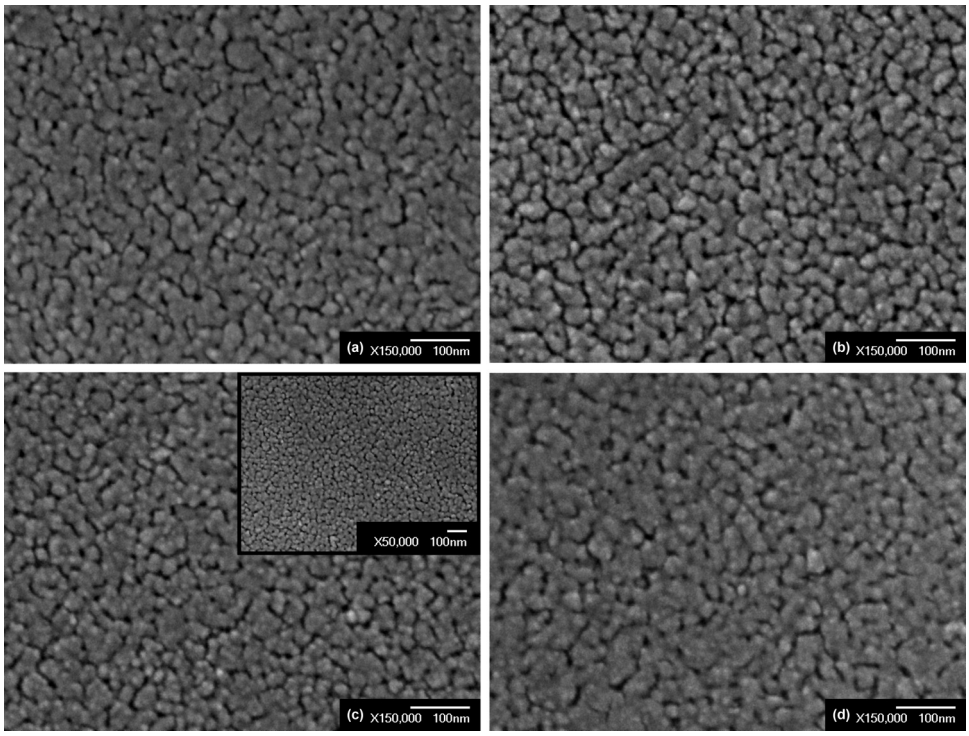

Fig. 2. SEM images of the 1× (a), 2× (b), (3×) (c) and (4×) (d) TiO_2 thin films deposited by sol–gel on Corning glass substrates at 600 °C.

disappearance rate (mol/min) and the formal quantum efficiency (FQE) for all TiO_2 thin films were calculated according to the methodology of Mills and Wang [18].

2.6. Photoelectrocatalytic study

The photoelectrocatalytic measurements were performed using a three-electrode electrochemical cell [25,26]. TiO_2 thin films on ITO glass substrates acted as the working electrode biased in the range between −1500 to +1000 mV. Ag/AgCl and Pt foils were employed as the reference and the counter-electrode, respectively. The measurements were carried out at a scan rate of 20 mV/s in dark and under UV illumination. Five UV-A-type lamps which predominantly emit at 365 nm (4 W, Philips TL 4W/08) were used as UV source with an incident light intensity of 0.7 mW/cm^2. Since the CH_3OH oxidation reaction produces carbonate via a CO intermediate, which gets strongly adsorbed on the active TiO_2 sites, thus reducing the catalytic efficiency of the oxide [27], 0.25 M sulfuric acid (H_2SO_4) was initially tested as an electrolyte solution with and without the presence of 0.5 M CH_3OH. However, the oxide was immediately removed in this electrolyte (i.e., TiO_2 was supernatant inside the cell). Hence, NaOH was finally chosen as the electrolyte solution at a concentration of 0.25 M, based on the literature [28–30].

3. Results and discussion

3.1. Structure

Fig. 1 depicts typical X-ray diffraction patterns of the TiO_2 thin films deposited by the sol–gel/spin-coating technique after 1, 3 and 4 spinning cycles at 600 °C with estimated thickness of ∼50–60 nm, ∼110–120 nm and ∼150 nm, respectively. In particular, the red solid line in Fig. 1a depicts the X-ray diffraction pattern of a 50-nm-thick (1×) TiO_2 thin film in which a single diffraction peak centered at 25.34° can only be observed. Similarly, Fig. 1b and c displays the X-ray diffraction patterns of 110-nm- (3×) and 150-nm-thick (4×) TiO_2 thin films deposited on Corning glass substrates under the same experimental conditions (green and blue solid lines in Fig. 1b and c, respectively). The diffraction peaks observed for the 4× TiO_2 thin films (25.34°, 37.84°, 48.18°, 54.02° and 55.12°) (see Fig. 1c) are in good agreement with the JCPDS card (No. 84-1286) for the crystal structure of anatase [31,13,32–35]. It can be observed that both 3× and 4× TiO_2 thin films show narrow XRD reflections with significantly higher intensity than the corresponding 1× TiO_2 sample, indicating, in general, enhanced crystallinity of the TiO_2 thin films with increasing thickness. Similar behavior was observed for the films grown at lower temperatures.

The mean crystallite dimensions (d) of the TiO_2 thin films were calculated using Scherrer's equation:

$$d = \frac{K\lambda}{(\beta^2 - {\beta_0}^2)^{1/2} \cos\theta} \quad (1)$$

where β is the measured broadening of a diffraction line peak at an angle of 2θ at half its maximum intensity (FWHM) in radians, β_0 is the instrumental broadening, $K = 180/\pi$, λ is the X-ray wavelength (0.154056 nm) and θ is the Bragg diffraction angle. By fitting the (101) diffraction peak to Scherrer's equation, crystallite size values were found to increase from 21.9 for 1× to 25.7 nm for 4× independent of deposition temperature.

3.2. Morphology

Fig. 2a–d illustrates the SEM images of the 50-nm- (1×), 70-nm- (2×), 110-nm- (3×) and 150-nm-thick (4×) TiO_2 thin films deposited by sol–gel on Corning glass substrates at 600 °C. As it can be observed, in all cases, the substrates were covered with crack-free, quite dense and uniform TiO_2 thin films. Similar observations are shown for the films grown at lower deposition periods (not shown here for brevity).

Fig. 3a–c presents AFM images (scan size 1 μm × 1 μm) of the 50-nm- (1×), 70-nm- (2×) and 110-nm-thick (3×) TiO_2 thin films

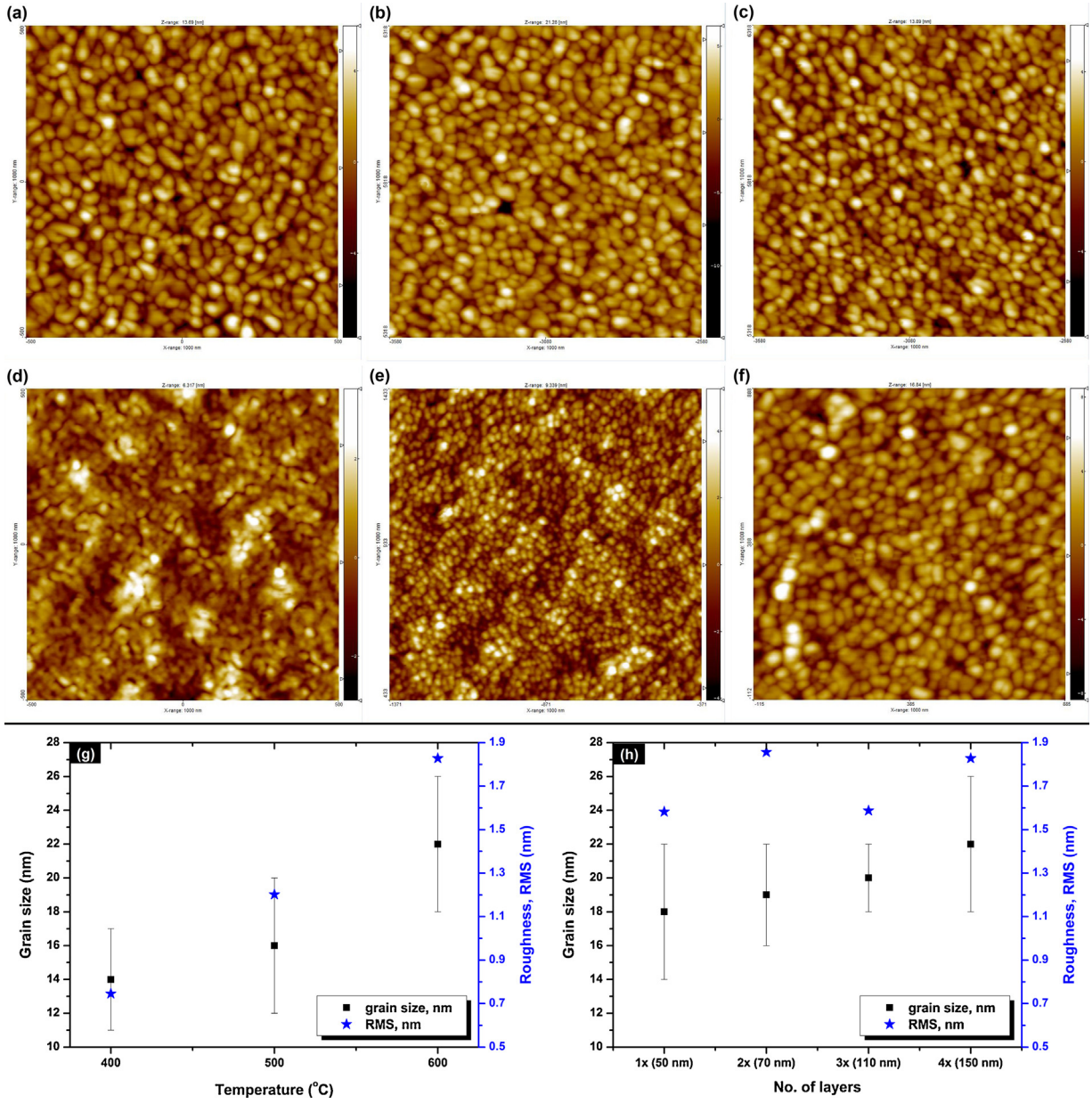

Fig. 3. (Top) AFM images (scan size 1 μm × 1 μm) of the 1× (a), 2× (b) and 3× (c) TiO_2 thin films deposited on Corning glass substrates via sol–gel at 600 °C and the 150-nm-thick (4×) TiO_2 thin films at 400 °C (d), 500 °C (e) and 600 °C (f), respectively. (Bottom) Grain size (black squares) and surface roughness (RMS, blue stars) of the as-grown TiO_2 thin films as a function temperature (g) and number of spin-coated layers (h) (For interpretation of the references to color in this figure legend and citation, the reader is referred to the web version of this article.)

deposited at 600 °C, while Fig. 3d–f illustrates the AFM images (scan size 1 μm × 1 μm) of the 150-nm-thick (4×) TiO_2 thin films at 400, 500 and 600 °C, respectively. It can be observed that all TiO_2 thin films are homogeneous, crack-free and densely packed, while their grains are significant small, exhibiting values of 14 ± 3 and 22 ± 4 nm for 4× TiO_2 thin films annealed at 400 and 600 °C, respectively. As it is shown in Fig. 2a–d and Fig. 3a–c and f, there is a good agreement between the results revealed from AFM and SEM analyses regarding the surface morphology of the sol–gel-deposited TiO_2 thin films.

Fig. 3g and h exhibits the variation in grain size (black squares) and surface roughness (RMS, blue stars) of the as-grown TiO_2 thin films as a function of annealing temperature (Fig. 3g) and number of spin-coated layers (Fig. 3h). From Fig. 3g, one can notice that for a fixed number of spinning cycles (4×, 150-nm-thick samples) the increase in annealing temperature from 400 to 600 °C leads to TiO_2 thin films with an RMS surface roughness ranging from ~0.8 to ~1.8 nm and a relatively small grain size variation from 14 ± 3 to 22 ± 4 nm, respectively. This behavior clearly demonstrates the stability of the as-grown sol–gel-deposited TiO_2 thin films for a wide range of annealing temperatures. Furthermore, similar conclusions arise for the 1× to 3× TiO_2 thin films deposited at 600 °C (see Fig. 3h) since the RMS surface roughness varies between ~1.6 and ~1.9 nm, while the grain size of the samples ranges from 18 ± 4 to 20 ± 2 nm.

One may then suggest that the RMS surface roughness is mainly dependent upon the annealing temperature and not the number of spinning cycles (film thickness), obtaining the maximum value at the highest annealing temperature (600 °C). Hence, we should expect at 600 °C, on the one hand, enhanced photocatalytic

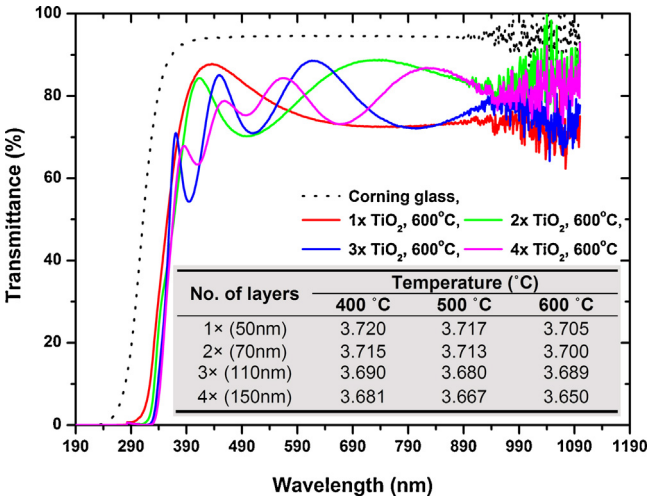

No. of layers	Temperature (°C)		
	400 °C	500 °C	600 °C
1× (50nm)	3.720	3.717	3.705
2× (70nm)	3.715	3.713	3.700
3× (110nm)	3.690	3.680	3.689
4× (150nm)	3.681	3.667	3.650

Fig. 4. Optical transmittance spectra of the 1× to 4× TiO_2 thin films grown at 600 °C in the wavelength region 190–1100 nm. In the inset, the optical energy bandgap (E_{gap}, eV) of the TiO_2 thin films, as determined using "Tauc" plots of α^2 as a function of $h\nu$.

performance since the adsorption of more water molecules will be promoted [36] and, on the other hand, improved electrooxidation behavior because there will be more defects for ions to enter the oxide [37].

3.3. Optical measurements

The optical transmittance spectra of the 1× to 4× TiO_2 thin films grown at 600 °C in the wavelength range of 190–1100 nm are presented in Fig. 4. All the TiO_2 thin films are highly transparent in the visible wavelength region with an average transmittance of about 75–90%, with a fall-off for wavelengths shorter than 350 nm.

The optical energy gap values (E_{gap}) of the TiO_2 thin films were determined by the extrapolation of the linear portion of $(\alpha h\nu)^2$ versus $h\nu$ plots ("*Tauc*" plots) (inset in Fig. 4). The values obtained for the as-deposited samples vary from 3.65 to 3.72 eV, similar to the ones reported by [38] and [39] for anatase TiO_2 thin films obtained by sol–gel approaches at 500 °C. The estimated values of the bandgap for the as-grown TiO_2 thin films are larger than bulk TiO_2 (3.3 eV), since the films consisting of fine crystallites show "blue shift" [40]. We assume that the increase in the bandgap is due to the quantum size effect (QSE), which occurs for semiconductor particles below 100 nm. Moreover, as seen in the inset of Fig. 4, the energy bandgap of the TiO_2 thin films generally decreases with annealing temperature and number of spinning cycles (film thickness). This decrease may be correlated with the grain size increase with annealing temperature, since when the latter increases, the defects and impurities tend to disappear causing a reorganization in the structure [40,41].

3.4. Photocatalysis

Fig. 5 presents the normalized integrated area vs. irradiation time curves for 1× to 4× TiO_2 thin films deposited by sol–gel on Corning glass at 400–600 °C. For comparison reasons, the photolysis curve (no catalyst present) is also displayed in the same figure.

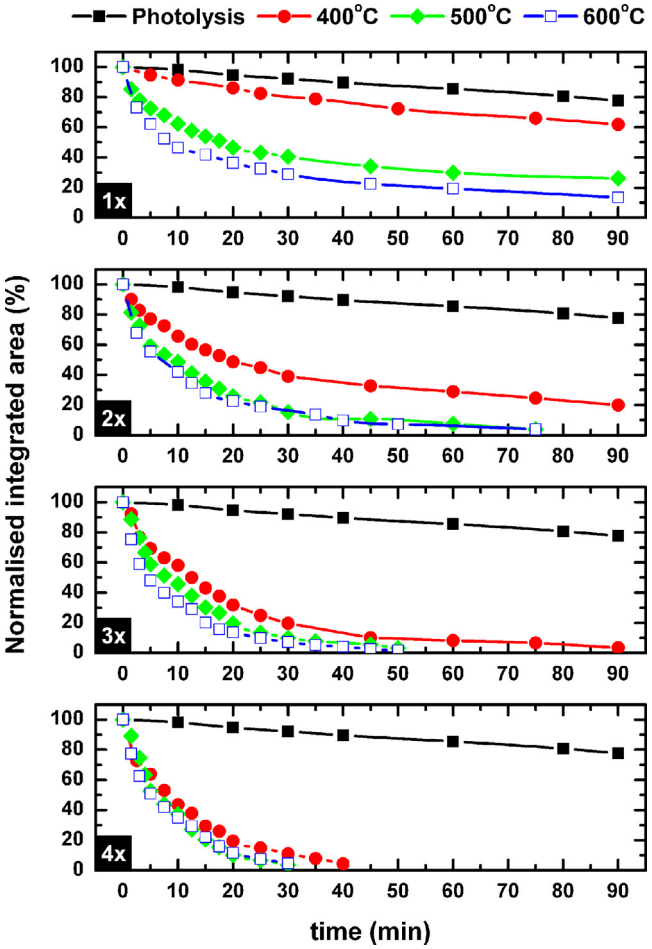

Fig. 5. Normalized integrated area vs. irradiation time for 1× to 4× TiO_2 thin films deposited by sol–gel on Corning glass at 400–600 °C. For comparison reasons, the photolysis curve (black solid squares) is also presented.

Table 1 summarizes the photocatalytic activity of TiO_2 thin films regarding the degradation of octadecanoic acid at 30 min exposure under UV-A illumination. Following the methodology explained by Mills and Wang [18] and Paz et al. [42], we found that the octadecanoic acid disappearance rate (mol/min) and the formal quantum efficiency (FQE) are the highest for the 150-nm-thick (4×) TiO_2 thin films deposited at 400–600 °C. In particular, the 4× TiO_2 thin film deposited at 400 °C shows an FQE value of $\sim 3.93 \times 10^{-3}$ and an octadecanoic acid disappearance rate of $\sim 3.71 \times 10^{-8}$ mol/min at 30 min, while the corresponding values for the films deposited at 500 and 600 °C are $\sim 4.43 \times 10^{-3}$/$\sim 4.18 \times 10^{-8}$ mol/min and $\sim 6.65 \times 10^{-3}$/$\sim 6.28 \times 10^{-8}$ mol/min, respectively. As one can notice from Table 1 (and the calculation of FQE and octadecanoic acid disappearance rate), the photocatalytic activity of all TiO_2 thin films regarding the % decomposition of octadecanoic acid is always significantly higher than that observed due to photolysis,

Table 1
Photocatalytic activity of the sol–gel-deposited TiO_2 thin films regarding the degradation of octadecanoic acid under UV-A illumination for 30 min.

Temperature (°C)	No. of layers			
	1× (50 nm)	2× (70 nm)	3× (110 nm)	4× (150 nm)
400 °C	20.14%	61.05%	80.39%	89.10%
500 °C	59.43%	84.68%	89.96%	96.41%
600 °C	71.09%	83.87%	92.74%	95.46%

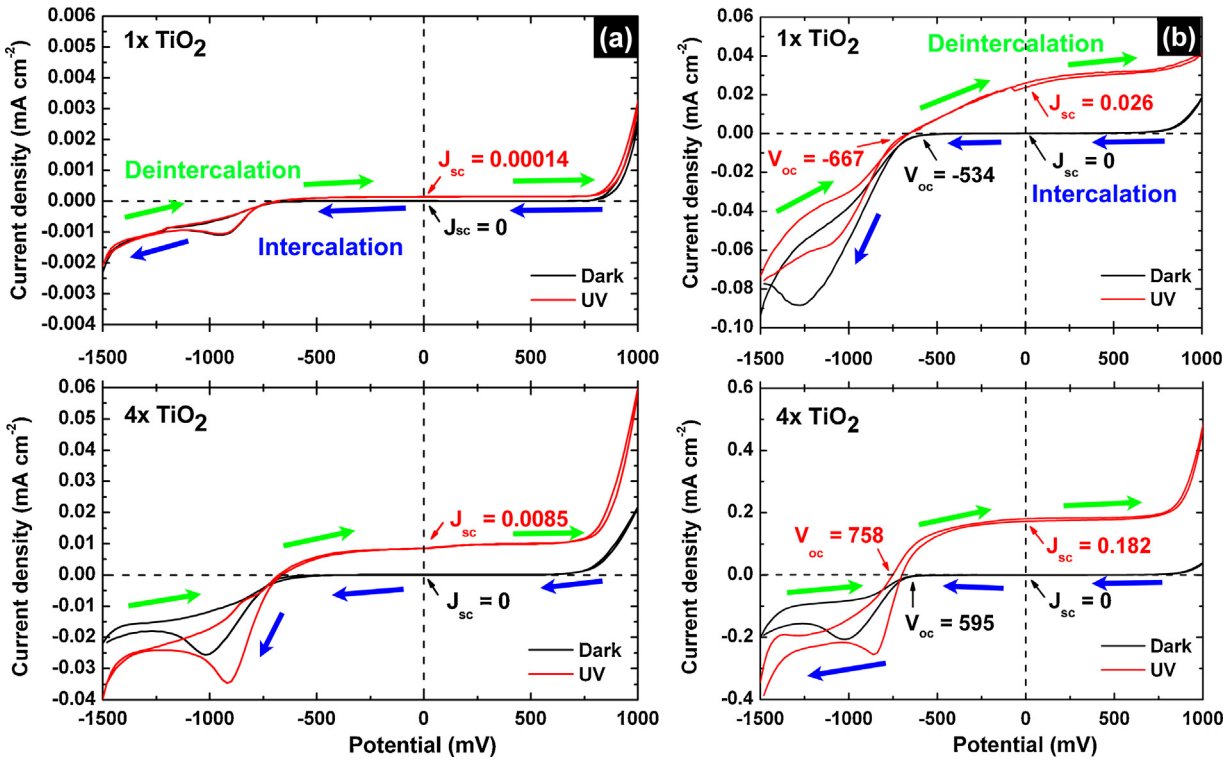

Fig. 6. Variation of current density with potential for the 1× and 4× TiO_2 thin films in dark and under UV illumination without (a) and with (b) the presence of methanol. Working electrode active surface area is 1 cm^2. Arrows with different colors are included to indicate the intercalation (cathodic) and deintercalation (anodic) regions (For interpretation of the references to color in this figure legend and citation, the reader is referred to the web version of this article.).

i.e., light irradiation of octadecanoic acid in the absence of a metal oxide catalyst. At 30 min, for example, the % octadecanoic acid degradation due to photolysis is only ~8%, reaching an FQE value of 0.05×10^{-3} and an octadecanoic acid disappearance rate of $\sim 4.44 \times 10^{-10}$ mol/min. Moreover, it should be noted that, our 150-nm-thick (4×) TiO_2 thin films annealed at 500 °C show photocatalytic activity (FQE = 6.65×10^{-3}) similar to the one reported by Paz et al. [42]. It can be generally concluded that the anatase TiO_2 thin films with the highest crystallinity exhibit the best photocatalytic performance, however, for maximum activity, a combination of high crystallinity and optimum grain size (at 500 °C) is required [43].

It is worth mentioning that the photocatalytic activity tests were carried out for at least five times on our TiO_2 samples in order to examine their stability under UV illumination, demonstrating no changes in the photocatalytic activity after five runs.

3.5. Photoelectrocatalytic evaluation

Based on the above analysis, we focused on studying the effect of spinning cycles (film thickness) on the electrooxidation performance of the films annealed at 500 °C via cyclic voltammetry experiments. The potential was ranged from −1500 to +1000 mV at a scan rate of 20 mV/s in 0.25 M NaOH (Fig. 6a) and 0.25 M NaOH + 0.5 M CH_3OH (Fig. 6b) in dark and under illumination for 1× and 4× TiO_2 thin films. Regarding the curves obtained in 0.25 M NaOH, they exhibit narrow cathodic peaks attributed to sodium intercalation in TiO_2. However, the process is irreversible since respective anodic peaks are not shown. In addition, those derived in the presence of methanol show similar behavior with the others, but with broad cathodic regions. The dark current was zero in all cases (see black curves in Fig. 6). However, the current density for the thin films under UV light illumination (red curves) was higher by two orders of magnitude in the presence of methanol, i.e., 0.0085 and 0.182 mA/cm^2 with and without methanol for the 4× TiO_2 films, respectively. The observed increase in the photocurrent is due to the efficient trapping of holes as also recorded with other alcohols [44].

Specifically, the generation of e^-/h^+ pairs can be promoted under UV illumination of TiO_2, which can in turn enhance methanol electrocatalysis. Holes will probably conduct the oxidation reactions (I) and (II) [45], since HO^- are very efficient hole scavengers.

$$6HO^- + 6h^+ \rightarrow 6HO\bullet \quad \text{(I)}$$

$$CH_3OH + 6HO\bullet \rightarrow CO_2 + 5H_2O \quad \text{(II)}$$

Combination of reactions (I) and (II) gives reaction (III), which is the most usual case in basic environments:

$$CH_3OH + 6HO^- + 6h^+ \rightarrow CO_2 + 5H_2O \quad \text{(III)}$$

While, the photogenerated electrons will drive the reduction reaction in the presence of oxygen as indicated in reaction (IV) [45]:

$$H_2O + 1/2O_2 + 2e^- \rightarrow 2OH^- \quad \text{(IV)}$$

It becomes evident from Fig. 6 that the current is lower in dark, while higher value is observed under UV illumination indicating that the TiO_2 films are photoactive [46]. The 4× TiO_2 presented the highest current value and consequently an enhanced photoactivity due to the crystalline anatase TiO_2 and the increased surface coverage of the substrate, which provides larger active volume for the alcohol oxidation.

The quantitative measure of the photoelectrocatalytic properties is the incident photon to current efficiency (ICPE, expressed in % [47]):

$$\text{IPCE}(\%) = \frac{1240 J_{sc}\ (\text{mA/cm}^2)}{\lambda\,(\text{nm}) \cdot P\,(\text{mW/cm}^2)} \times 100$$

where J_{sc} is the recorded short-circuit current density for a monochromatic incident power density P and λ is the wavelength of the incident radiation. Thus for $P = 0.7\ mW/cm^2$ peaking at 365 nm and current density of $0.182\ mA/cm^2$, the IPCE value is 88.3% for the 4× sample in the presence of methanol. In addition, the fill factor of the same sample was calculated using the formula [44]:

$$FF = \frac{(J \cdot V)_{max}}{J_{sc} \cdot V_{oc}}$$

where J_{sc} is the short-circuit current density, V_{oc} the open-circuit voltage and $(J{\cdot}V)_{max}$ is the maximum value of the $J{\cdot}V$ as depicted from Fig. 6. In this case, J_{sc}, V_{oc} and $(J{\cdot}V)_{max}$ are $0.182\ mA/cm^2$, 595 mV, and $0.055\ mW/cm^2$, hence FF = 0.51. The IPCE and FF values are comparable [44,45,47,48], while in some cases higher than others [49,50]. These discrepancies may be related with the methanol concentration and the pH of the electrolyte.

4. Conclusions

TiO_2 thin films were grown on glass substrates via a sol–gel procedure at 400–600 °C. The only detectable crystal structure is the one of anatase, while the grain size of the as-grown thin films varies from 14 ± 3 to 22 ± 4 nm. All TiO_2 thin films are highly transparent in the visible wavelength region and show remarkable photocatalytic activity regarding the % conversion of octadecanoic acid, with the 4× TiO_2 thin film at 500 °C presenting the highest activity (FQE = 6.65×10^{-3} at 30 min). We suggest that this is related to both the crystalline anatase TiO_2 phase and the optimum grain size of the film. In addition, the current recorded in the presence of methanol is larger than in its absence due to the efficient trapping of holes. The crystallinity and the surface coverage of the titania films are important factors for the efficient methanol oxidation.

Acknowledgements

This project is implemented through the Operational Program "Education and Lifelong Learning", Action Archimedes III and is co-financed by the European Union (European Social Fund) and Greek National Funds (National Strategic Reference Framework 2007–2013).

References

[1] A. Fujishima, X. Zhang, D.A. Tryk, Surf. Sci. Rep. 63 (2008) 515.
[2] K. Hashimoto, H. Irie, A. Fujishima, Jpn. J. Appl. Phys. 44 (2005) 8269.
[3] M. Pelaez, N.T. Nolan, S.C. Pillai, M.K. Seery, P. Falaras, A.G. Kontos, P.S.M. Dunlop, J.W.J. Hamilton, J.A. Byrne, K. O'Shea, M.H. Enterazi, D.D. Dionysiou, Appl. Catal. B 125 (2012) 331.
[4] P. Pichat (Ed.), Photocatalysis and Water Purification, Wiley-VCH, Weinheim, 2013.
[5] M.A. Henderson, Surf. Sci. Rep. 66 (2011) 185.
[6] L. Lopez, W.A. Daoud, D. Dutta, Surf. Coat. Technol. 2 (15) (2010) 251.
[7] C. Sanchez, J. Livage, M. Henry, F. Babonneau, J. Non. Crystal. Sol. 100 (1988) 65.
[8] M. Rahman, G. Yu, T.S. Soga, T. Jimbo, H. Ebisu, M. Umeno, J. Appl. Phys. 88 (2000) 4634.
[9] J. Yuan, S. Tsujikawa, J. Electrochem. Soc. 142 (1995) 3444.
[10] P. Kajitvichyanukul, et al., Sci. Technol. Adv. Mater. 6 (2005) 352.
[11] L. Sun, et al., Sep. Purif. Technol. 68 (2009) 83.
[12] G.Y. Li, et al., Appl. Catal. B 140–141 (2013) 225.
[13] A. Rampaul, I.P. Parkin, S.A. O'Neill, J. DeSouza, A. Mills, N. Elliott, Polyhedron 22 (2003) 35.
[14] B.E. Yoldas, J. Mater. Sci. 21 (1986) 1087.
[15] G. Kenanakis, D. Vernardou, E. Koudoumas, N. Katsarakis, J. Crystallogr. Growth 311 (2009) 4799.
[16] G. Kenanakis, D. Vernardou, N. Katsarakis, Appl. Catal. A 411 (2012) 7.
[17] M. Suzuki, T. Ito, Y. Taga, Appl. Phys. Lett. 78 (2001) 3968.
[18] A. Mills, J. Wang, Photochem. Photobiol. A 182 (2006) 181.
[19] D. Vernardou, G. Kalogerakis, E. Stratakis, G. Kenanakis, E. Koudoumas, N. Katsarakis, Solid State Sci. 11 (2009) 1499.
[20] D. Vernardou, E. Stratakis, G. Kenanakis, H.M. Yates, S. Couris, M.E. Pemble, E. Koudoumas, N. Katsarakis, J. Photochem. Photobiol. A 202 (2009) 81.
[21] J. Shang, W. Li, Y. Zhu, J. Mol. Catal. A Chem. 202 (2003) 187.
[22] A. Mills, N. Elliott, I.P. Parkin, S.A. O'Neill, R.J. Clark, J. Photochem. Photobiol. A Chem. 151 (2002) 171.
[23] H.M. Yates, M.G. Nolan, D.W. Sheel, M.E. Pemble, J. Photochem. Photobiol. A Chem. 179 (2006) 213.
[24] M.R.S. Castro, E.D. Sam, M. Veith, P.W. Oliveira, Nanotechnology 19 (2008) 105704.
[25] D. Vernardou, P. Paterakis, H. Drosos, E. Spanakis, I.M. Povey, M.E. Pemble, E. Koudoumas, N. Katsarakis, Sol. Energ. Mater. Sol. C 95 (2011) 2842.
[26] D. Vernardou, A. Sapountzis, E. Spanakis, G. Kenanakis, E. Koudoumas, N. Katsarakis, J. Electrochem. Soc. 160 (2013), D6.
[27] C. Bianchini, P.K. Shen, Chem. Rev. 109 (2009) 4183.
[28] C. Jia, H. Yin, H. Ma, R. Wang, X. Ge, A. Zhou, X. Xu, Y. Ding, J. Phys. Chem. C 113 (2009) 16138.
[29] H. Zhang, W. Zhou, Y. Du, P. Yang, C. Wang, J. Xu, Int. J. Hydrogen Energ. 35 (2010) 13290.
[30] H. Cao, Z. Wang, G. Hou, G. Zheng, Surf. Coat. Technol. 205 (2010) 885.
[31] Y. Takahashi, Y. Matsuoka, J. Mater. Sci. 23 (1988) 2259.
[32] Y. Ohya, J. Mishina, T. Matsuda, T. Ban, Y. Takahashi, J. Am. Ceram. Soc. 82 (10) (1999) 2601.
[33] H. Yu, J. Yu, B. Cheng, M. Zhou, J. Solid State Chem. 179 (2006) 349.
[34] L. Miao, S. Tanemura, S. Toh, K. Kaneko, Masaki Tanemura, J. Crystallogr. Growth 264 (2004) 246.
[35] K.K. Saini, S.D. Sharma, M. Chanderkant, D. Kar, C.P. Singh, Sharma, J. Non-Crystallogr. Solids 353 (2007) 2469.
[36] O. Zywitzki, T. Modes, P. Frach, D. Glöss, Surf. Coat. Technol. 202 (2008) 2488.
[37] H. Drosos, A. Sapountzis, E. Koudoumas, N. Katsarakis, D. Vernardou, J. Electrochem. Soc. 159 (2012), E145.
[38] B.-H. Kim, J.-H. Ahn, J.-H. Jeong, Y.-S. Jeon, K.-O. Jeon, K.-S. Hwang, Ceram. Int. 32 (2006) 223.
[39] T. Giannakopoulou, T. Vaimakis, S. Ladas, C. Trapalis, N. Todorova, J. Sol. Energy Eng. 130 (2008) 041007.
[40] T. Wang, H. Wang, P. Xu, X. Zhao, Y. Liu, S. Chao, Thin Solid Films 334 (1998) 103.
[41] Mustafa Öztas, Chin. Phys. Lett. 25 (2008) 4090.
[42] Y. Paz, Z. Luo, L. Rabenberg, A. Heller, J. Mater. Res. 10 (1995) 2842.
[43] Q. Zhang, J.-B. Joo, Z. Lu, M. Dahl, D.Q.L. Oliveira, M. Ye, Y. Yin, Nano Res. 4 (2011) 103.
[44] M. Antoniadou, P. Lianos, Appl. Catal. B 99 (2010) 307.
[45] Panagiotis Lianos, J. Hazard. Mater. 185 (2011) 575.
[46] R.R. Dickinson, D.L. Battye, V.M. Linton, P.J. Ashman, G.J. Nathan, Int. J. Hydrogen Energy 35 (2010) 1329.
[47] M. Antoniadou, P. Bouras, N. Strataki, P. Lianos, Int. J. Hydrogen Energy 33 (2008) 5045.
[48] M. Antoniadou, D.I. Kondarides, D. Labou, S. Neophytides, P. Lianos, Sol. Energy Mater. Sol. Cells 94 (2010) 592.
[49] K. Drew, G. Girishkumar, K. Vinodgopal, P.V. Kamat, J. Phys. Chem. B 109 (2005) 11851.
[50] Z. Zhang, Y. Yuan, Y. Fang, L. Liang, H. Ding, G. Shi, L. Jin, J. Electroanal. Chem. 610 (2007) 179.